RARE SIGNALS DETECTION IN NONWHITE NOISE ENVIRONMENT BASED ON MULTIDIMENSIONAL SIGNAL SUBSPACE FOR HYPERSPECTRAL IMAGE

S. Bourennane and C. Fossati

Ecole Centrale Marseille, Université Aix-Marseille,
Institut Fresnel CNRS-UMR 7249, France

ABSTRACT

Due to the resolution limitation of the hyperspectral imaging sensors, some targets only take one or two pixels in the hyperspectral image (HSI). These targets are called small targets. When HSI is impaired and has to be denoised, small targets might be suppressed in the denoising process, which can degrade the detection performance. In this paper, we propose a method to improve the small target detection performance of HSI which is damaged by nonwhite thermal noise. One recently proposed nonwhite noise reduction algorithm prewhitening-multiway-Wiener-Filter (PMWF) and a usually used spatial-domain wavelet packet transform with SureShrinkage (SWPT-SURE) denoising approach are compared with the algorithm proposed in this paper. Finally, a real-world HYDICE HSI is employed to investigate the noise whitening capability and the improvement of small target detection performance.

Index Terms— Hyperspectral image, Target detection, nonwhite noise, multiway filtering, wavelet packet transform.

1. INTRODUCTION

A hyperspectral image (HSI) contains not only spatial information of but also spectral signatures of objects, therefore it is a suitable tool for detecting targets on the ground. However, owning to the limited spatial resolution of the hyperspectral imaging sensor, some objects on the ground only have a spatial extent in the order of the sensor geometrical resolution [1]. These objects are called small targets in this paper. It is a challenging problem to detect the small targets especially when noise in HSI is considered. In fact, HSI is always impaired by noise from radiation, atmospheric scattering and thermal noise in the acquiring instrument. Reducing noise and emphasizing target contribution is a common approach to solve the target detection problem in noise environment. For HSI, there are two main noise sources: the signal-independent thermal noise, and the signal-dependent photonic noise. In this paper, we mainly focus on reducing signal-independent noise.

The classical denoising methods rearrange HSI into a matrix whose columns contain the spectral signatures of all the pixels and the signal subspace is estimated by methods based on the analysis of second-order-statistics (SOS), such as PCA. Since these methods need to know the rank of the signal subspace, some rank estimation algorithms relying on SOS have been developed, such as the classical Akaike information criterion(AIC) and the recent noise whitened Harsanyi-Frarrand-Chang (NWHFC) algorithm [2]. However, the main problem of the SOS-based-techniques is their weakness in preserving small targets [1]. Concerning the small-target-preservation problem, Kuybeda has proposed the Maximum Orthogonal Complement Analysis algorithm (MOCA) and Acito has presented the Robust Signal Subspace Estimation algorithm (RSSE) [3]. These two methods assume that the small targets have a high residual energy on the subspace that is orthogonal to the background one. However, this assumption is not always fulfilled. The spatial information preserves a spectrum with a particular spatial characteristics. To jointly use spatial and spectral information, a multiway Wiener filter (MWF) [4] is proposed to denoise HSI as a whole entity based on TUCKER3 decomposition. In MWF, the filter in each mode is computed as a function of filters in the other modes, which reflects its capability in jointly utilizing information in each mode of HSI. Since MWF is proposed for white noise, a prewhitening MWF (PMWF) method [5] is proposed to make it applicable under the more generalized signal-independent nonwhite thermal noise model.

Though MWF performs well in denoising HSI, since it treats HSI as a whole entity, the large and small targets cannot be separated, therefore the small ones might be suppressed [6] . Distinguishing from MWF, wavelet transform (WT) can separate small targets and large targets into different coefficient sets, therefore it is possible to treat these two types of targets with different parameters to better preserve the small ones. SureShrink is a commonly used denoising method in the wavelet domain. Recently, a hybrid spatial-spectral noise-reduction (HSSNR) algorithm was proposed to reduce noise in spectral derivative domain and a combination of PCA and wavelet shrinkage was proposed to reduce noise in the last several PCA-output-channels. However, these methods only consider white noise, which does not conform to the noise in HSI [7].

In this paper, we investigate the jointly component filtering algorithm(MWPT-MWF), to make it applicable in the

978-0-9928-6265-7/16/$31.00 ©2016 IEEE

signal-independent nonwhite noise environment and show its capability of preserving small targets in the denoising process. For the nonwhite noise environment, we present a component-based prewhitening method, which can whiten noise in each component adaptively. Concerning the capability of preserving small target, the proposed method will be compared with PMWF and spatial-domain wavelet packet transform with SureShrink(SWPT-SURE) [8] in the performance of target detection for a real-world data.

The remainder of the paper is as follows: Section 2 introduces some basic knowledge about multilinear algebra. Section 3 introduces the signal model. Section 4 shows the proposed method in reducing nonwhite noise. Section 5 presents some experimental results and finally section 6 concludes this paper.

2. MULTILINEAR ALGEBRA TOOLS

2.1. n-mode unfolding

$\mathbf{X}_n \in \mathbb{R}^{I_n \times M_n}$ denotes the n-mode unfolding matrix [5] of a tensor $\mathcal{X}$The columns of $\mathbf{X}_n$ are the I_n-dimensional vectors obtained from $\mathcal{X}$ by varying index i_n while keeping the other indices fixed. Here, we define the n-mode rank K_n as the n-mode unfolding matrix rank,that is K_n = rank$(\mathbf{X}_n)$.

2.2. n-mode product

The n-mode product [5] is defined as the product between a data tensor $\mathcal{X} \in \mathbb{R}^{I_1 \times I_2 \times \ldots I_N}$ and a matrix $\mathbf{B} \in \mathbb{R}^{J \times I_n}$ in mode n. It is denoted by $\mathcal{C} = \mathcal{X} \times_n \mathbf{B}$.

3. SIGNAL MODEL

A noisy multidimensional data is modeled as a tensor $\mathcal{R} \in \mathbb{R}^{I_1 \times I_2 \times I_3}$ resulting from a multidimensional signal $\mathcal{X} \in \mathbb{R}^{I_1 \times I_2 \times I_3}$ impaired by an additive noise $\mathcal{N} \in \mathbb{R}^{I_1 \times I_2 \times I_3}$. The tensor $\mathcal{R}$ can be expressed as:

$$\mathcal{R} = \mathcal{X} + \mathcal{N} \tag{1}$$

In this paper, only thermal noise is considered, which means that noise is independent from the signal and the noise in each band is zero mean Gaussian white noise while noise variance changes from band to band,

4. COMPONENT-BASED NONWHITE NOISE REDUCTION

4.1. SWPT for separating targets

As the large and small targets are different in the spatial size, SWPT is applied to separate different target sizes. For the convenience in expressing 3D HSI, SWPT is written in tensor form as

$$\mathcal{C}^{\mathcal{R}} = \mathcal{R} \times_1 \mathbf{W}_1 \times_2 \mathbf{W}_2 \tag{2}$$

and the corresponding reconstruction:

$$\mathcal{R} = \mathcal{C}^{\mathcal{R}} \times_1 \mathbf{W}_1^T \times_2 \mathbf{W}_2^T \tag{3}$$

where $\mathbf{W}_n \in \mathbb{R}^{I_n \times I_n}, n = 1,2,3$ indicate the wavelet packet transform matrices. The transform level vector is $\mathbf{l} = [l_1, l_2]^T$, where $l_n \geq 0$ denotes the wavelet packet transform level in mode n. Being named a component of scale $\mathbf{m} = [m_1, m_2]$ in this paper, the coefficient tensor $\mathcal{C}^{\mathcal{R}}{}_{\mathbf{l},\mathbf{m}}$ can be extracted by:

$$\mathcal{C}^{\mathcal{R}}{}_{\mathbf{l},\mathbf{m}} = \mathcal{C}^{\mathcal{R}} \times_1 \mathbf{E}_{m_1} \times_2 \mathbf{E}_{m_2} \tag{4}$$

and the corresponding inverse process is:

$$\mathcal{C}^{\mathcal{R}} = \sum_{m_1} \sum_{m_2} \mathcal{C}^{\mathcal{R}}_{\mathbf{l},\mathbf{m}} \times_1 \mathbf{E}_{m_1}^T \times_2 \mathbf{E}_{m_2}^T \tag{5}$$

where the extraction operator $\mathbf{E}_{m_n}$ is defined as:

$$\mathbf{E}_{m_n} = [\mathbf{0}_1, \mathbf{I}_{\frac{I_n}{2^{l_n}} \times \frac{I_n}{2^{l_n}}}, \mathbf{0}_2] \in \mathbb{R}^{I_n/2^{l_n} \times I_n} \tag{6}$$

where $\mathbf{0}_1$ is a zero matrix with size $\frac{I_n}{2^{l_n}} \times \frac{m_n I_n}{2^{l_n}}$ and $\mathbf{0}_2$ is a zero matrix with size $\frac{I_n}{2^{l_n}} \times \frac{(2^{l_n}-1-m)I_n}{2^{l_n}}$.

4.2. Nonwhite noise reduction

The signal coefficient tensor $\mathcal{C}^{\mathcal{X}}_{\mathbf{l},\mathbf{m}}$ [8]can be estimated by filtering $\mathcal{C}^{\mathcal{R}}_{\mathbf{l},\mathbf{m}}$ with MWF. However, MWF is proposed for the white noise situation [9], therefore $\mathcal{C}^{\mathcal{R}}_{\mathbf{l},\mathbf{m}}$ should be whitened before being filtered by MWF. In [8], noise in $\mathcal{R}$ is whitened before MWPT. After MWPT the noise in the component $\mathcal{C}^{\mathcal{R}}_{\mathbf{l},\mathbf{m}}$ is nonwhite For this reason, we propose a component based noise prewhitening method

$$\mathcal{C}^{\mathcal{N}}_{\mathbf{l},\mathbf{m}} = \mathcal{N} \times_1 \mathbf{W}_1 \times_2 \mathbf{W}_2 \times_1 \mathbf{E}_{m_1} \times_2 \mathbf{E}_{m_2} \tag{7}$$

Unfolding $\mathcal{C}^{\mathcal{N}}_{\mathbf{l},\mathbf{m}}$ in mode-3, we can obtain:

$$\mathbf{C}^{\mathcal{N}}_{\mathbf{l},\mathbf{m}} = \mathbf{N}_3[(\mathbf{E}_{m_1}\mathbf{W}_1)^T \otimes (\mathbf{E}_{m_2}\mathbf{W}_2)^T] \tag{8}$$

where $\mathbf{N}_3$ is the mode-3 unfolding form of $\mathcal{N}$. Furthermore, the noise covariance matrix of $\mathbf{C}^{\mathcal{N}}_{\mathbf{l},\mathbf{m}}$ can be obtained:

$$E\left[\mathbf{C}^{\mathcal{N}}_{\mathbf{l},\mathbf{m}}(\mathbf{C}^{\mathcal{N}}_{\mathbf{l},\mathbf{m}})^T\right] = E\left[\mathbf{N}_3 \xi {\mathbf{N}_3}^T\right] \tag{9}$$

where

$$\begin{aligned}\xi &= [(\mathbf{E}_{m_1}\mathbf{W}_1)^T \otimes (\mathbf{E}_{m_2}\mathbf{W}_2)^T][(\mathbf{E}_{m_1}\mathbf{W}_1) \otimes (\mathbf{E}_{m_2}\mathbf{W}_2)] \\ &= [(\mathbf{E}_{m_1}\mathbf{W}_1)^T(\mathbf{E}_{m_1}\mathbf{W}_1)] \otimes [(\mathbf{E}_{m_2}\mathbf{W}_2)^T(\mathbf{E}_{m_2}\mathbf{W}_2)]\end{aligned}$$

If the support length of wavelet is less than $I_n/2^{l_n}$, we can obtain that $(\mathbf{E}_{m_n}\mathbf{W}_n)^T(\mathbf{E}_{m_n}\mathbf{W}_n) = \mathbf{I}_{I_n/2^{l_n} \times I_n/2^{l_n}}$. As a

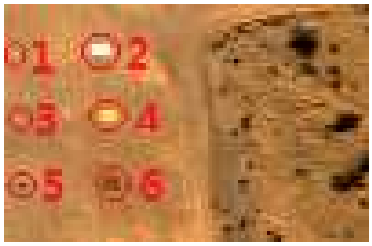

(a) Ground-truth map

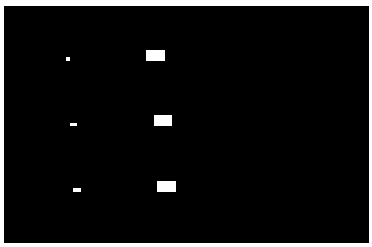

(b) Mask

Fig. 1. Real-world data.

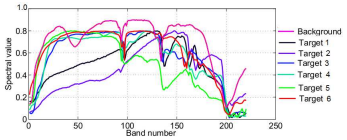

Fig. 2. Spectral signatures of the 6 targets

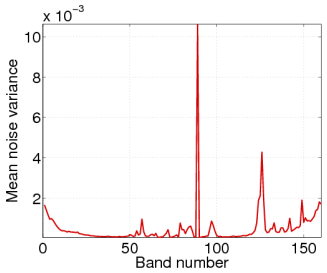

Fig. 3. Mean noise variance in each band (SNR=17dB)

result, $\xi = \mathbf{I}_{I_1\times I_1} \otimes \mathbf{I}_{I_2\times I_2} = \mathbf{I}_{(I_1I_2)\times(I_1I_2)}$. By substituting ξ into (9), we can obtain:

$$E\left[\mathbf{C}^{\mathcal{N}}_{\mathbf{l},\mathbf{m}}(\mathbf{C}^{\mathcal{N}}_{\mathbf{l},\mathbf{m}})^T\right] = E\left[\mathbf{N}_3\mathbf{N}_3{}^T\right] \tag{10}$$

As described in [5], $E\left[\mathbf{N}_3\mathbf{N}_3{}^T\right]$ can be estimated by the multiple regression theory. Therefore, equation (10) implies that $E\left[\mathbf{C}^{\mathcal{N}}_{\mathbf{l},\mathbf{m}}(\mathbf{C}^{\mathcal{N}}_{\mathbf{l},\mathbf{m}})^T\right]$ can be estimated by that theory as well:

$$E\left[\mathbf{C}^{\mathcal{N}}_{\mathbf{l},\mathbf{m}}(\mathbf{C}^{\mathcal{N}}_{\mathbf{l},\mathbf{m}})^T\right] = \text{diag}\{\sigma^2_{\mathbf{m},1},\ldots,\sigma^2_{\mathbf{m},I_3}\} \tag{11}$$

where $\sigma_{\mathbf{m},i_3} = \rho^2_{\mathbf{m},i_3}(1-\tau^2_{\mathbf{m}i_3})$ and $\rho^2_{\mathbf{m},i_3}$ is the i_3-th diagonal element of the sample covariance matrix [5] of $\mathbf{C}^{\mathcal{N}}_{\mathbf{l},\mathbf{m}}$ and $\tau^2_{\mathbf{m},i_3}$ is the multiple correlation coefficient of band i_3 on the other I_3-1 bands. Accordingly, the noise whitening matrix of $\mathbf{C}^{\mathcal{R}}_{\mathbf{l},\mathbf{m}}$ is:

$$\mathbf{G} = \text{diag}\{\sigma^{-1}_{\mathbf{m},1},\ldots,\sigma^{-1}_{\mathbf{m},I_3}\} \tag{12}$$

By considering the prewhitening process, $\mathbf{C}^{\mathcal{X}}_{\mathbf{l},\mathbf{m}}$ can be estimated by:

$$\begin{aligned}\hat{\mathcal{C}}^{\mathcal{X}}_{\mathbf{l},\mathbf{m}} =& \mathcal{C}^{\mathcal{R}}_{\mathbf{l},\mathbf{m}} \times_3 \mathbf{G} \times_1 \mathbf{H}_{1,\mathbf{m}} \times_2 \mathbf{H}_{2,\mathbf{m}} \times_3 \mathbf{H}_{3,\mathbf{m}} \\ =& \mathcal{C}^{\mathcal{R}}_{\mathbf{l},\mathbf{m}} \times_1 \mathbf{H}_{1,\mathbf{m}} \times_2 \mathbf{H}_{2,\mathbf{m}} \times_3 (\mathbf{G}\mathbf{H}_{3,\mathbf{m}})\end{aligned} \tag{13}$$

where $\mathbf{H}_{n,\mathbf{m}}$ is the mode-n MWF filter.

Henceforth, for the sake of compactness, the proposed algorithm is called SWPT-CPMWF.

5. EXPERIMENTAL RESULTS

In this section, we use a real-world high spatial resolution data acquired by HYperspectral Digital Imagery Collection Experiment (HYDICE). The HYDICE image contains 65 rows, 100 columns and 160 spectral bands, and is modeled as a $65 \times 100 \times 160$ tensor in this paper. Six targets of interest are selected in the image as shown in the ground-truth map in Fig. 1(a) and the corresponding mask is shown in Fig. 1(b). The 6 targets are chosen because they have different spectral signatures and sizes, so that the detection performance on different target sizes can be evaluated.

Signal-independent nonwhite noise is added into HSI according to the model in (1), with the noise variance in each band shown in Fig. 3. Concerning the simulation parameters, we considered SNR ranged from 15 to 25 dB (with a step of 2 dB) to reproduce different detection scenarios. Moreover, wavelet db3 is selected to do SWPT with transform levels $[l_1, l_2] = [1, 1]$.

5.1. Noise-whitening performance evaluation and comparison

The relationship given in (10) is important in this paper because it gives a way to estimate the noise covariance matrix of each component. To validate this relationship, Fig. 4 shows the noise-variance-estimate curves of every component and HSI dataset. As is evident, there are only small variations among these curves, which implies that it is efficient of estimating noise variance in each component by multiple regression theory. The small variations among the curves reflect that the noise variance estimate calculated by using data in the component can adapt better to the component itself than that calculated by using HSI.

To emphasize the whitening result explicitly, Fig. 5 presents the normal probability plot for the noise not whitened and the corresponding whitened noise in each component. As is shown in Fig. 5(a), the values of noise not whitened do not follow a straight line, which means that the noise not

whitened cannot be considered as coming from a normally distributed dataset. Hence the prewhitening operation is necessary to obtain white noise. The first way coming into our view is to whiten $\mathcal{R}$ before SWPT, also named HSI-based prewhitening method. Fig. 5(b) presents the noise values in each component, which is obtained by HSI-based prewhitening method. It is evident that only the noise in component [1 1], the finest scale coefficient set, can be considered as normally distributed, but noise in the other components does not follow normal distribution. Fig. 5(b) implies that HSI-based prewhitening method is not a suitable solution for whitening noise in each component. As a result, the component-based prewhitening method is designed in this paper. As is presented in Fig. 5(c), the noise in each component is approximately normally distributed after being whitened by the component-based prewhitening method. The comparison in Fig. 5 implies that the proposed algorithm is efficient in whitening noise in the component.

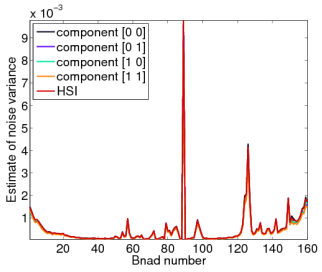

Fig. 4. Estimate of noise variance in each band, SNR=17dB

5.2. Target-detection performance evaluation and comparison

Spectral Angle Mapper (SAM) detector is used in the experiments to detect targets in the image. As SAM does not require the characterization of background, it can avoid inaccuracy of the comparison result caused by the noise covariance matrix estimation error. The SAM detector can be expressed as:

$$\mathrm{T}_{\mathrm{SAM}}(\mathbf{x}) = \frac{\mathbf{s}^T\mathbf{x}}{(\mathbf{s}^T\mathbf{s})^{1/2}(\mathbf{x}^T\mathbf{x})^{1/2}} \tag{14}$$

where $\mathbf{s}$ is the reference spectrum, and $\mathbf{x}$ is the pixel spectrum. To assess the performances of detection, the probability of detection (Pd) is defined as:

$$\mathrm{Pd} = \frac{\sum_i^{n_s} N_i^{rd}}{\sum_i^{n_s} N_i} \tag{15}$$

and the probability of false alarm (Pfa) is defined as:

$$\mathrm{Pfa} = \frac{\sum_i^{n_s} N_i^{fd}}{\sum_i^{n_s} (I_1 \times I_2 - N_i)} \tag{16}$$

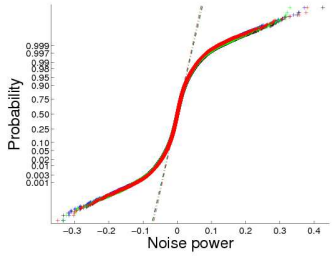

(a)

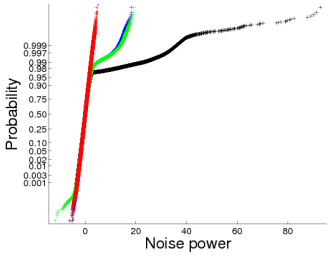

(b)

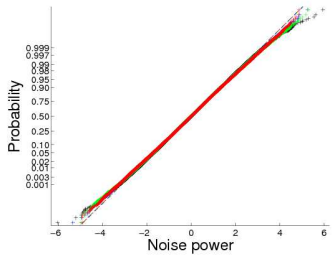

(c)

Fig. 5. Normal probability plot for noise in each component (a) noise not whitened and (b) noise whitened by HSI-based method (c) noise whitened by component-based method, SNR=17dB.

where n_s is the number of spectral signatures, N_i the number of pixels with spectral signature i, N_i^{rd} the number of rightly detected pixels, and N_i^{fd} the number of falsely detected pixels.

Apart from the detection performance for each target, most of the time, we consider more about the detection performance for all the targets in HSI. In the scenario where small and large targets coexist, an outstanding denoising method should preserve both of them to improve the target detection performance. Fig. 6 supplies Pd versus SNR curves of all the targets after denoising by different methods. These results are strongly in favor of the proposed method SWPT-CPMWF. The excellent performance of SWPT-CPMWF is due to its capability of preserving both small targets and large ones while reducing noise from HSI. PMWF cannot preserve small target with weak power, therefore its Pd is less than SWPT-CPMWF. SWPT-SURE [8] suppress the small target in the denoising process due to its global SureShrink, which degrades its performance. Though the avoiding denoising raw data can preserve small target well, the noise in the data prevents from detection the large target with small power, therefore Pd in this case is less than the ones after denoising by the three methods.

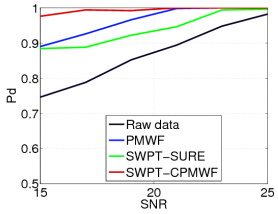

Fig. 6. Pd versus SNR curves of all the targets with Pfa=10^{-4} after denoising by $SWPT-SURE$, PMWF and $SWPT-CPMWF$ in various noise environment

6. CONCLUSION

In this paper we have proposed an automatic denoising algorithm SWPT-CPMWF which can be utilized directly in the signal-independent nonwhite noise environment. To process the nonwhite noise, SWPT-CPMWF takes a component-based noise-whitening method, which makes it data-adopting. Moreover, not like most denoising algorithms that cannot preserve small targets, the proposed SWPT-CPMWF performs well in preserving small targets even when targets of different sizes coexist in the same HSI. The capability of preserving small target makes SWPT-CPMWF a suitable tool for improving target detection efficiency in the noise environment. A real-world HSI data HYDICE is used in the experiments to test the performance of the proposed SWPT-CPMWF. In the noise-whitening experiment, we have compared the HSI-based prewhitening method and the proposed component-based prewhitening method, and the result is strongly in favor of the latter one. Furthermore, different denoising methods are also compared in the aspect of improving target detection performance. From the detection result, it is evident that the proposed SWPT-CPMWF outperforms the other denoising methods in detecting both large and small targets.

REFERENCES

[1] N. Acito, M. Diani, and G. Corsini, "Hyperspectral signal subspace identification in the presence of rare signal components," *IEEE Trans. Geosci. Remote Sens.*, vol. 48, no. 4, pp. 1940–1954, 2010.

[2] I. C. Chein and D. Qian, "Estimation of number of spectrally distinct signal sources in hyperspectral imagery," *IEEE Trans. Geosci. Remote Sens.*, vol. 42, no. 3, pp. 608–619, 2004.

[3] S. Bourennane, C. Fossati, and A. Cailly, "Improvement of classification for hyperspectral images based on tensor modeling," *IEEE Trans. Geosci. Remote Sens. Letters*, vol. 7, no. 4, pp. 801–805, Oct. 2010.

[4] D. Muti and S. Bourennane, "Survey on tensor signal algebraic filtering," *Signal Process.*, vol. 87, no. 2, pp. 237–249, Feb. 2007.

[5] X. Liu, S. Bourennane, and C. Fossati, "Nonwhite noise reduction in hyperspectral images," *IEEE Geosci. Remote Sens. Lett.*, vol. 9, no. 3, pp. 368–372, 2012.

[6] S. Bourennane, C. Fossati, and A. Cailly, "Improvement of target-detection algorithms based on adaptive three-dimensional filtering," *IEEE Trans. Geosci. Remote Sens.*, vol. 49, no. 4, pp. 1383–1395, 2011.

[7] X. Liu, S. Bourennane, and C. Fossati, "Denoising of hyperspectral image using parafac model and statistical performance analysis," *IEEE Trans. on Geoscience and Remote Sensing*, vol. 50, no. 10, pp. 3717–3724, 2012.

[8] T. Lin and S. Bourennane, "Hyperspectral image processing by jointly filtering wavelet component tensor," *IEEE Trans. on Geoscience and Remote Sensing*, vol. 51, no. 6, pp. 3529–3541, 2013.

[9] D. Letexier, S. Bourennane, and J. Talon, "Nonorthogonal tensor matricization for hyperspectral image filtering," *IEEE Trans. Geosci. Remote Sens. Letters*, vol. 5, no. 1, pp. 3–7, 2008.